Nationaal Lucht- en Ruimtevaartlaboratorium
National Aerospace Laboratory NLR

NLR-TP-98007

Development of a metal test box configuration to test a range of skin panels of a composite horizontal stabilizer

J.C.F.N. van Rijn and H.G.S.J. Thuis

DOCUMENT CONTROL SHEET

	ORIGINATOR'S REF.		SECURITY CLASS.
	TP 98007		Unclassified

ORIGINATOR
National Aerospace Laboratory NLR, Amsterdam, The Netherlands

TITLE
Development of a metal test box configuration to test a range of skin panels of a composite horizontal stabilizer

PUBLISHED IN
Composite Structures by Elsevier Applied Science

AUTHORS	DATE	pp	ref
J.C.F.N. van Rijn and H.G.S.J. Thuis	980108	28	1

DESCRIPTORS

Aircraft structures	Nastran	Structural analysis
Bending	Panels	Twisting
Composite materials	Reinforcing fibers	
Composite structures	Stabilizer	
Finite element method	Stiffening	
Load tests	Strain measurement	

ABSTRACT

Within the framework of a national technology programme under a contract awarded by the Netherlands Agency for Aerospace Programmes (NIVR), a composite stabilizer was developed by Fokker Aircraft B.V. in close collaboration with NLR. One of the activities in this technology program for NLR was to develop a test box for testing large composite skin panels and to test the composite panels on this box. The main goals of this part of the program were:

- To develop a single test box on which a number of test panels with different configurations could be loaded to relatively high strain levels without incurring damage to the test box;
- To load the test panels in such a way that an optimum correspondence between strain distributions in the test panels and the horizontal stabilizer skins was attained;
- To validate the design concepts of the skin panels by comparison of calculated and measured strain distributions.

All objectives have been met successfully.

- Six different panels were tested on a single metal test box. The panels were loaded up to a maximum of 3.0 times Limit Load with a total of 21 different loading conditions without incurring any damage to the metal test box.
- The loading of the test panels was such that an acceptable correspondence of the measured strain distributions and the calculated strain distributions in the horizontal stabilizer skins was attained.
- The measured strain distributions compared quite well with the calculated strain distributions for the test panels.

Contents

24 Figures

(28 pages in total)

Development of a metal test box configuration to test a range of skin panels of a composite horizontal stabilizer

J.C.F.N. van Rijn and H.G.S.J. Thuis
National Aerospace laboratory, Structures Department, Voorsterweg 31, 8316 PR Marknesse, The Netherlands

Within the framework of a national technology programme under a contract awarded by the Netherlands Agency for Aerospace Programmes (NIVR), a composite stabilizer was developed by Fokker Aircraft B.V. in close collaboration with NLR. One of the activities in this technology program for NLR was to develop a test box for testing large composite skin panels and to test the composite panels on this box. The main goals of this part of the program were:

- To develop a single test box on which a number of test panels with different configurations could be loaded to relatively high strain levels without incurring damage to the test box;
- To load the test panels in such a way that an optimum correspondence between strain distributions in the test panels and the horizontal stabilizer skins was attained;
- To validate the design concepts of the skin panels by comparison of calculated and measured strain distributions.

All objectives have been met successfully.

- Six different panels were tested on a single metal test box. The panels were loaded up to a maximum of 3.0 times Limit Load with a total of 21 different loading conditions without incurring any damage to the metal test box.
- The loading of the test panels was such that an acceptable correspondence of the measured strain distributions and the calculated strain distributions in the horizontal stabilizer skins was attained.
- The measured strain distributions compared quite well with the calculated strain distributions for the test panels.

1 Introduction

Under a contract awarded by the Netherlands Agency for Aerospace Programmes (NIVR), a national technology programme was carried out in close collaboration between Fokker Aircraft B.V. and the National Aerospace Laboratory. The goal of this technology programme was to develop the technology required to design, fabricate and certify a carbon fibre reinforced plastic (CFRP) horizontal stabilizer. To achieve this goal the building block approach was used [Ref. 1].

In this building block approach all aspects were addressed starting at the material level (by testing thousands of small coupons), through a large number of small components (e.g. by testing hundreds of small skin panel and spar details), to sub-assemblies of increasing complexity, up to the level of a complete torsion box of the composite stabilizer.

Large composite skin panels were among the larger sub-assemblies to be developed. The panels were designed and manufactured by Fokker Aircraft B.V. and tested by NLR. Four different panel configurations were tested which were representative for skin panels of the upper and lower skin and encompassed the centre and root section of the stabilizer skin panels. The panel tests were primarily meant to validate the design concepts used in the root section.

To test these large composite skin panels in a correct way it was deemed necessary to mount the panels on a box structure in order to get a realistic build-up of the bending and torsional moments towards the centre section of the panels.
This paper addresses the development of the metal test box and the methodology to determine the actuator input loads. In addition panel test results, obtained during the box tests, are compared to finite element calculations.

The definition of the composite skin panels in relation to the composite horizontal stabilizer skins are briefly discussed. The test box concept and test set-up are explained in detail. The finite element modelling technique of the test box and the composite skin panels is presented. The use of finite element analysis to obtain loading conditions for the test box is presented. The test programme is briefly described. The comparison of some experimental results with finite element analysis results is given. Finally, some conclusions are drawn.

2 The development of the test box

The objectives of the test box programme were:

- To develop a single metal test box on which a number of composite skin panels with different configurations could be loaded up to failure without causing damage to the metal test box.
- To determine the actuator loads to load the test panels in the same way as the composite horizontal stabilizer.

2.1 The test panels

The main load carrying component of the horizontal stabilizer is the horizontal stabiliser torsion box. The main components of the torsion box are the upper and lower skins, the aft, rear and auxiliary spars and the ribs. The torsion box comprises composite front, rear and auxiliary spars

with L-stiffeners, dimpled metal ribs, sandwich composite ribs and several metal fittings.

The skin panels were stiffened by blade stiffeners which were cobonded to the skin laminate. At the transition of the inboard and outboard parts of the panels, stiffener run-outs were used in combination with doublers.

Four different test panel configurations were tested on the metal test box which were derived from the lower and upper skins of the composite horizontal stabilizer (Lower Aft, Lower Front, Upper Aft and Upper Front). Their locations relative to the skin panels of the composite stabilizer are shown in figure 1.

A detailed view of one of the test panels is given in figure 2. The test panels were made of unidirectional carbon/epoxy prepreg tape HTA/6376. All test panels except for the Lower Front panel, were configured with an inspection hole at the root of the panel (see Fig. 2). All edges of the test panels were reinforced with tabs to allow a proper load introduction.
The Aft test panels were configured with a rearward extension, which functions as an elevator support in the composite horizontal stabilizer.

2.2 The metal test box concept

In figure 3 a view of the metal test box is given, in which the various parts are named. Figure 4 gives a cross sectional view of the box, with a test panel attached.

The metal test box contains steel spar simulations and steel rib simulations, which support the test panels and provide for a build-up of the strains in the test panels towards the centre section, as well as a steel bottom plate (see Fig. 3).

The metal test box was configured with steel ribs for lower as well as upper skin panels. In this way four different skin panels could be loaded on the same metal test box. The rib simulations to be used with the aft-panels are indicated with “a” in figure 3, the rib simulations to be used with the front-panels are indicated with “b”.

The composite test panels were connected to the metal test box using aluminium parts. The edges of the test panels were connected to the steel spar simulation of the metal test box by angle sections. The test panels were connected to the metal rib simulations by aluminium ribs as shown in figure 4.

One of the problems which had to be solved was to avoid permanent deformation or even failure of the metal test box when loading the test panels up to failure. Therefore the spars of the metal test box were configured with slits (see Fig. 5), which allowed the test panel to be deformed up

to relatively high strain levels, while keeping the metal test box relatively unaffected in case of a loading in bending.

However, in case of a test panel failure in tension, this spar concept might still lead to permanent damage in the metal test box. Therefore, the spars of the metal test box were equipped with chains (see Figs. 5 and 6). Each spar was equipped with two steel chains: one inside and one outside the metal test box. The chains have slotted holes. These slotted holes allow the metal test box to deform to a certain degree. If the deformation of the metal test box exceeds this level, the slotted holes of the chains will begin to pick up loads and hence the chains will limit the deformation of the metal test box.

In case of a composite panel failure in compression, the slits in the spars are configured so that they will make contact with each other and hence will limit the deformation of the metal test box. Figure 6 shows a detail of the slit spar of the metal test box, the location of the chain at the outside of the spar and the aluminium angle sections which are used to connect the composite skin panels to the metal test box.

Figure 7 shows the top view of the complete metal test box. The figure clearly shows the locations of the chains. The different rib locations can also be seen. Two rigid steel bars are connected to the end of the metal test box. By connecting hydraulic actuators at the end of these bars the required bending moments can be applied to the composite skin panels.

2.3 The metal test box test set-up

The metal test box was connected to a rigid frame. Loads were introduced to the metal test box by six hydraulic actuators: five positioned vertically (F_{z1}, F_{z2}, F_{z3}, F_{z5} and F_{z6} see Fig. 8) and one positioned horizontally (Fy1 see Fig. 8). The loads of actuators F_{z1} and F_{z2} were introduced at the end of the box through two beams. Elevator loads were introduced to the aft panels by a dead weight using a mechanism (see Figs. 8 and 9).

3 Finite Element Models

Finite element analyses were performed using MSC NASTRAN version 67.5 (Ref. 2), of the metal test box configuration including the composite test panels, as well as of the composite horizontal stabilizer. In this section the finite element models of the composite horizontal stabiliser, of the metal test box and of the test panels are described.

3.1 Composite horizontal stabilizer model

The finite element model of the composite horizontal stabilizer is shown in figure 10.

The finite element model contains 2444 nodes, 2667 4-node quadrilateral or 3-node triangular shell elements and 1262 beam elements.

3.2 Test box model

A top view of the finite element model of the test box (looking inside the box) is shown in figure 11. The finite element model contains 1147 nodes, 1002 4-node-quadrilateral shell elements and 14 2-node-beam elements.

The dimensions of the finite element model of the box were dictated by the dimension of the panels, since test box and panel finite element models were to be connected.

A further description of some of the parts, which are indicated in figure 3, are given in the next sections.

3.2.1 Finite element models of spar simulations

The actual spar configuration and its finite element representation are shown in figure 12. The actual design of the spar simulations is too complicated to be incorporated in the finite element model. Since the large slits will accommodate virtually all displacement, these are modelled with double nodes.

3.2.2 Finite element models of rib simulations

In figure 4 a cross section of the test box is given. It was deemed necessary to incorporate the actual height of the aluminium rib, because the stiffness of the combined rib simulations is dominated by the stiffness of the aluminium part. In the finite element model the height of the aluminium rib is the distance between the top of the spar simulation and the top of the rib simulation.

3.2.3 Applied loads and boundary conditions

The applied loads and boundary conditions for the finite element model are indicated in figure 13.

The nodal forces F_{z1}, F_{z2}, F_{z3}, F_{z5} and F_{z6} act in the direction of the positive z-axis. The nodal force F_{z3} acts on the location indicated by load 4a in figure 4 for the aft panels and on the location indicated by 4b for the forward panels.
The nodal force F_{y1} acts in the direction of the positive global y-axis.

All displacements are constrained for the 14 nodes at the upper and lower edge of the support plate.

3.3 Test panel models

In this section the modelling techniques which were used for the test panel shell and beam elements, and for the connection between the test panel and the test box are given.

In order to facilitate the comparison between the strain distributions of the stabilizer and the test panels, the element sizes in stringer direction for the panel finite element model were copied from the finite element model of the stabilizer.

The finite element model of the Lower-Aft panel contained 270 nodes, 226 shell elements and 99 beam elements. The finite element model for the connection between the test panel and the test box contained 54 shell elements and 92 beam elements.
The finite element models for the other test panels and their connection to the box contained a similar number of nodes and elements.

3.3.1 Panel shell elements

The skin material of the panels is modelled in 4-node shell elements. The shell elements in the finite element model of the Lower-Aft panel are shown in figure 14. The distribution of the various material properties is indicated.

The finite element model of the panel is placed on the top plane of the finite element model of the test box. The distance between the reference plane of the panel shell elements and the actual mould surface of the panel was taken into account by using an offset for the plate elements.

As first and as last ply in the finite element model a 0.001 mm thick ply was added with a ply orientation in the direction of the stringer, to facilitate the determination of surface strains in the stringer direction and perpendicular to the stringer direction for post-processing purposes.

3.3.2 Panel beam elements

As in the composite horizontal stabilizer finite element model, the panel stringers are modelled using beam elements. The beam elements in the finite element model of the Lower-Aft panel are shown in figure 15.

The stringers are placed on the skin. As in the stabilizer finite element model, the shear centre of the beam elements is located at the interface between skin and stringer. The offset of the beam elements, which is given in the global coordinate system, is therefore the offset of the skin minus the local thickness of the skin.

The location of the neutral axis of the stringer is specified relative to this offset point. The stringer is furthermore characterized by its cross sectional area, and moments of inertia in two directions. A Young's modulus and a shear modulus are given for the stringer material.

3.3.3 Finite element model of the connection between the test panels and the metal test box

The panels are connected to the metal test box by aluminium angle sections.

An overview of the finite element model of the connection is given in figure 16. The aluminium angle sections connecting the panel and the rib simulations are modelled by 4-node shell elements. The aluminium angle sections connecting the panel and the spar simulations are modelled by 2-node beam elements.

The connection between the finite element model of the panel and the finite element model of the spar simulations is shown schematically in figure 17. The construction of connecting beam elements was necessary because the test box and the panel finite element models are not compatible, which resulted in the finite element models having only incidentally common nodes. All nodes which are connected, are situated at the line along the top of the spar simulation. The beam elements connect all panel nodes on this line and those spar simulation nodes on this line which are located in between two slits.

4 Determination of actuator forces

The configurations of the test panels are based on the configurations of the upper and lower skins of the composite horizontal stabilizer. The loading conditions of the test panels should result in similar strain conditions as computed by finite element analyses for the composite horizontal stabilizer skins. To achieve this, a combination of actuator forces had to be determined which gave an optimum correspondence between strains in the stabiliser skins and strains in the test panels.

4.1 Methodology

The strain distribution in the composite horizontal stabilizer was determined for a number of critical load cases, representing extreme loading conditions, using finite element analysis. Also, a finite element analysis of the test set-up was performed, in which the contribution of the six actuators to the strain distribution in the test panels was determined individually.

The optimum combination of actuator loads was determined by least square minimisation of the difference between test panel and stabilizer strains in the skin for a number of relevant elements, using the maximum load of the actuators as constraints. The selected relevant elements for the

Lower-Aft panel are indicated in figure 14.

The correspondence of the normal strains in stringer direction was deemed more important than the correspondence of the shear strains, and the correspondence of strains at one location was considered more important than at another location. For instance, the correspondence of the strains directly outboard of rib 2 (locations 1 and 2 in Fig. 14) was deemed more important than at the centre section (locations 3 and 4 in Fig. 14).

Moreover, it should be noted that in the test set-up strains perpendicular to the stringer direction cannot be induced independently: strains in this direction occur only as a result of Poisson's contraction. In the stabilizer, loads perpendicular to the stringer direction do occur. Strains perpendicular to the stringer direction were therefore not taken into account in the determination of the actuator forces.

4.2 Results

The individual actuator load contributions to the strains in the Lower-Aft panel are given in figure 18. The location numbers refer to the elements as indicated in figure 14. The values given pertain to a load per actuator of 10 kN.
Most salient is the large difference in contribution of F_{z1}, F_{z2} and F_{z3} on the one hand and F_{y1}, F_{z5} and F_{z6} on the other. The contributions of the former are more than ten times larger than that of the latter. In this respect, it should be noted that the actuators F_{z5} and F_{z6} are positioned quite close to the support, and that most of the load of actuator F_{y1} is carried by the bottom of the metal test box.
The contributions of the various actuators to the strain distribution in the other test panels were very similar to that of the Lower-Aft panel.

The strain in stringer direction for a particular load case is shown in figure 19.a for the finite element model of the lower skin as part of the composite horizontal stabilizer. The strain in stringer direction of the Lower-Aft test panel for this load case, as obtained using the optimum combination of actuator loads, is given in figure 19.b. As can be seen, the correspondence of composite horizontal stabilizer and test panel strains is quite good, particularly in the vicinity of the root section.

It was established that with the given actuator configuration it was possible to generate a wide range of normal and shear strain distributions in the test panels. Ultimately, for all panels and all load cases (21 different loading conditions in total) a satisfactory combination of actuator loads was established.

5 The test programme

Four different test configurations were tested (see Fig. 1): Lower Aft, Lower Front, Upper Aft and Upper Front. Two more panels of the Lower Aft configuration were tested, which contained details relevant to either damage tolerance behaviour or repair design.
Several combinations of actuator loads were applied to each panel. Each combination of actuator loads was representative for a particular load case, either symmetric or asymmetric. Loads were applied in discrete load steps. After each load step the applied loads, the deformation and the strains were recorded.

All panels, but the damage tolerance panel, were statically tested up to 2.05 times Limit Load at ambient conditions, in order to demonstrate the capability to witstand Ultimate Load. An environment knock down factor of 1.35 was used to compensate for the fact that the tests were carried out at ambient conditions.
None of the panels failed. Subsequently, a number of panels were loaded up to 3 times Limit Load.

In total, 21 different loading conditions were applied to the six panels. The maximum panel strain level in the vicinity of the spar was approximately 5000 μstrain both in tension and in compression, without incurring damage to the metal test box. Clearly, the test box design proved to be satisfactory.

5.1 Panel instrumentation

The panel instrumentation comprised Linear Variable Displacement Transducers (LVDT's), internal displacement transducers in the actuators, strain gauge rosettes and single strain gauges.

The instrumentation plan of the lower-front panel is shown in figure 20. The strain gauge rosettes were mainly applied in pairs, one on the outside side (Fig. 20.a) and one on the stringer side of the panel (Fig. 20.b). A number of single strain gauges was applied in a similar manner. Single strain gauges were used to obtain information with regard to the strain distribution in a stringer cross section. The location of the strain gauges on the stringer cross section is shown in cross section A-A in 20.c. The direction of the three rosette strain gauges a, b, and c are perpendicular to the stringers, under an angle of 45° and parallel with the stringers, respectively.

6 Comparison of experimental and finite element calculation results

The experimental results were compared to the finite element results which were obtained for actual loading conditions.

In the discussion of the results, the load is expressed in a non-dimensional form by J, the load factor. For the Design Limit Load the load factor is equal to 1, for Design Ultimate Load the load factor is equal to 1.5. The experimental results and the finite element results are divided by the load factor J. In this way the non-linearity of the strains with increasing load is readily visualised, and a single curve suffices to show the corresponding finite element results.

6.1 Processing and presentation of strains

The strain gauge results can be grouped in such a way that the strain distribution along a line on the test panel is shown. As an example, the results for the Lower-Front panel along two lines are presented:

- Line 1 parallel to the rear spar simulation and located in between the doubler and the first stringer near the rear spar. At this line 6 pairs of strain gauge rosettes and 1 pair of single strain gauges (inside and outside) are located.
- Line 2 along the second stringer at the front side of the panel. At this line, 3 stringer strain gauge combinations are located.

For each line the strain gauge results are presented as a function of the distance along the line.

The strains in the shell elements are the strains as calculated for the first and last layers in the stacking sequence of an element. These layers were 0.001 mm thick dummy layers with a fibre direction parallel to the stringer direction. Strains are evaluated in the centre of each element. The curve showing the finite element results simply connects these results. It should be kept in mind that inboard of rib 2 the differences between the strains of the elements are attributable mainly to the difference in material thickness, which was a more or less stepwise increase.

The strains for a pair of rosettes are presented as average and bending strains in stringer direction ε_x, perpendicular to the stringer direction ε_y, and the corresponding shear strain ε_{xy}. The average and bending strains ε^{avg} and ε^{bend} were calculated from the strains on the inside (ε^i) and the outside (ε^o) of the test panel, using:

$$\varepsilon^{avg} = \frac{\varepsilon^i + \varepsilon^o}{2}$$
$$\varepsilon^{bend} = \frac{\varepsilon^i - \varepsilon^o}{2} \qquad (1)$$

The shear strain for one rosette was first calculated from the rosette strains using:

$$\varepsilon_{xy} = \varepsilon_b - \frac{\varepsilon_a + \varepsilon_c}{2} \qquad (2)$$

in which ε_a, ε_b and ε_c are the strains in the three rosette strain gauges. The average and twisting shear strains for the pair of rosettes were calculated subsequently.

The stringer deformations comprised the strain at the neutral axis ε_{na}, and the curvatures with respect to the local coordinate system ϕ_y and ϕ_z. The stringer deformations were computed directly from element forces and moments of the stringers, using:

$$\varepsilon_{na}=\frac{N}{E\cdot A} \quad \phi_z=\frac{M_1}{E\cdot I_1} \quad \phi_y=\frac{M_2}{E\cdot I_2} \qquad (3)$$

in which E is the Young's modulus of the stringer material, which was computed using the stringer lay-up and the ply elasticity parameters. The x-axis in the stringer coordinate system is oriented along the stringer axis, the z-axis is normal to the skin surface, and the y-axis completes an orthogonal x, y, z coordinate system.
The strain ε at any location in the beam can be calculated from the stringer deformations ε_{na}, ϕ_y and ϕ_z using:

$$\varepsilon=\varepsilon_{na}-\phi_z\cdot(y-y_{na})-\phi_y\cdot(z-z_{na}) \qquad (4)$$

in which y and z indicate the position, at which the strain is calculated, and y_{na} and z_{na} indicate the position of the neutral axis of the beam. These coordinates are given in the beam element coordinate frame. For each beam element the strains are given for both nodal points. Therefore two results are given for each node, resulting in a jagged appearance of the curves.

The strains obtained with the strain gauges were also converted to stringer deformations ε_{na}, ϕ_y and ϕ_z.

6.2 Comparison of results

The experimental results are shown for a number of load factors.
The finite element results for the test panel and for the composite horizontal stabilizer are also indicated.

6.2.1 Strain comparison for skin

The scaled average and bending strains in stringer direction between the doubler and the stringer near the rear spar ε_x^{avg} and ε_x^{bend}, for the strain gauges along line 1 are shown in figure 21.
The experimental ε_x^{avg} strains compare quite well with the calculated strains for the finite element model of the panel test set-up.
The calculated ε_x^{bend} strains are negligible, however there is little correspondence with the experimental ε_x^{bend}.
As can be seen, the correspondence between the results for finite element models of the composite horizontal stabilizer and the panel test set-up is quite good.

The scaled average strain perpendicular to the stringer direction ε_y^{avg} and the average shear strains ε_{xy}^{avg} for the strain gauges along line 1 are given in figure 22.

The experimental ε_y^{avg} and ε_{xy}^{avg} both compare quite well with the calculated strains for the finite element model of the panel test set-up.
The results for the stress component ε_y^{avg} for the finite element models of the composite horizontal stabilizer and for the panel test set-up are different. As was mentioned in section 4.1 strains perpendicular to the stringer direction cannot be induced independently in the test panels, and were therefore not taken into account in the actuator load optimisation. The results for the strain component ε_{xy}^{avg} match for some elements but are quite different in between.

6.2.2 Strain comparison for stringer

The scaled strain at the neutral axis of the stringer ε_{na} and the scaled curvatures ϕ_y and ϕ_z along the second stringer at the front side of the panel are shown in figures 23 and 24.

The experimental ε_{na} compare quite well with the calculated strains for the finite element model of the panel test set-up.
The experimental and calculated ϕ_y and ϕ_z are rather different.

Again, the correspondence between the results for finite element models of the composite horizontal stabilizer and the panel test set-up is quite good.

6.3 Discussion

The calculated ε_x^{avg}, ε_y^{avg} and ε_{xy}^{avg}, as well as ε_{na} compare quite well overall with the experimental values.

The experimental bending and twisting behaviour of the skin and the stringers was found to be quite different from the calculated values. It should be noted that all nodes in the panel finite element model are connected to the shell elements, which model the skin, and to the beam elements, which model the stringers. This means that the deformation of the shell and beam elements of the panel is completely interdependent both in bending and extension. The magnitude of the calculated scaled bending strains perpendicular to the stringer direction ε_y^{bend} and of the calculated scaled twisting shear strain ε_{xy}^{twist} is quite small. The deformation of the skin in between two stringers, which is characterised by a quasi-symmetry condition at each stringer, can not be described within a single 4-node element.

The calculated distribution of ε_x^{avg} and ε_{xy}^{avg} for the composite horizontal stabilizer and the panel test set-up finite element models compared quite well, the distribution of ε_y^{avg} was different for each model. For both models the magnitudes of the bending and twisting strains were limited.

It can be concluded that the required realistic build-up of the bending and torsional moments towards the centre section of the panels was achieved.

7 Conclusions

A metal test box was succesfully developed. On the metal test box six different panels were tested. The panels were loaded up to a maximum of 3.0 times Limit Load with a total of 21 different loading conditions without incurring any damage to the metal test box. The metal test box provided for the required realistic build-up of the bending and torsional moments towards the centre section of the panels.

The experimental average strains and the average strains calculated for the panel test set-up compared quite well in most cases.

The experimental bending and twisting strains were different from the bending and twisting strains calculated for the panel test set-up.

The calculated distribution of ε_x^{avg} and ε_{xy}^{avg} for the composite horizontal stabilizer and the panel test set-up finite element models compared quite well, the distribution of ε_y^{avg} was different for each model. For both models the magnitudes of the bending and twisting strains were limited.

8 References

1 **Rouchon, J.**, “Certification of large airplane composite structures, recent progress and new trends in compliance philosophy”, ICAS-90-1.8.1 (1990).

2 MSC/NASTRAN, Quick Reference Guide (version 67), The Mac Neal-Schwendler Corporation, 1992.

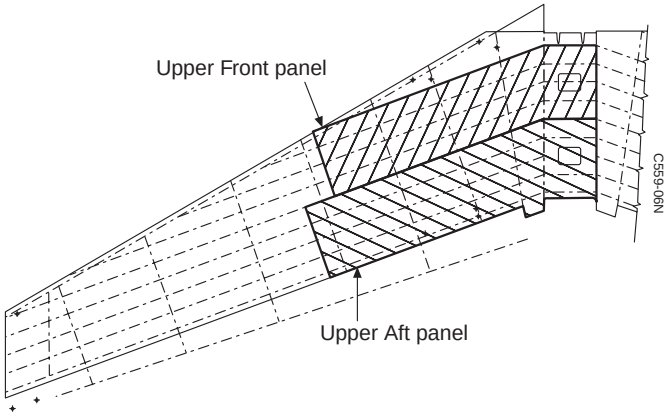

a) Lay-out of upper skin

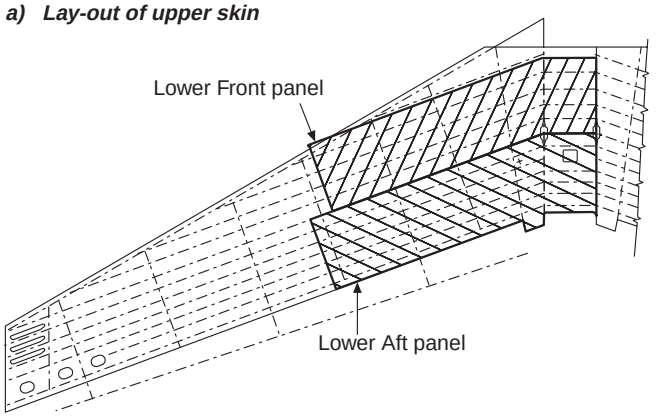

b) Lay-out of lower skin

Fig. 1 Lay-out of skins and locations of test panels

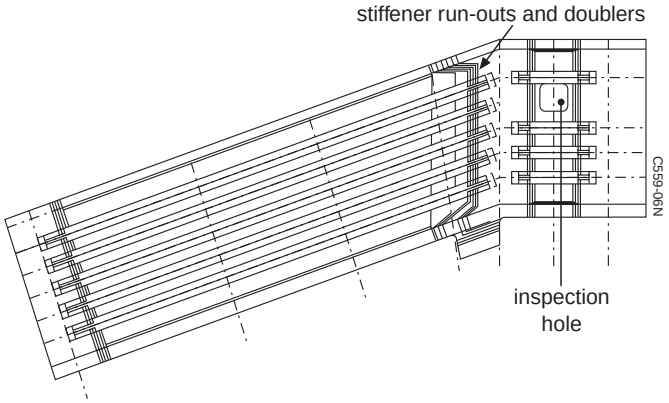

Fig. 2 Lower Aft test panel

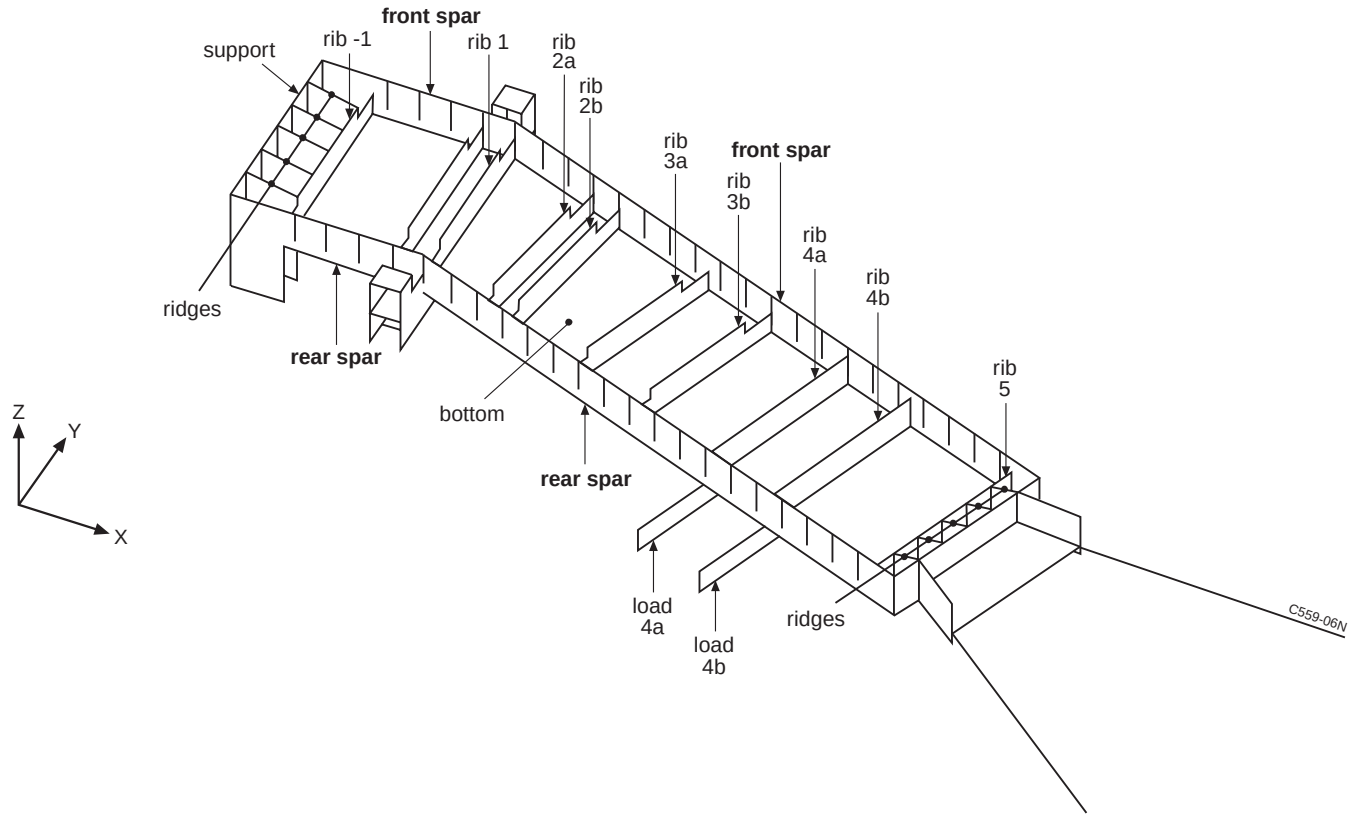

Fig. 3 Metal test box configuration and nomenclature

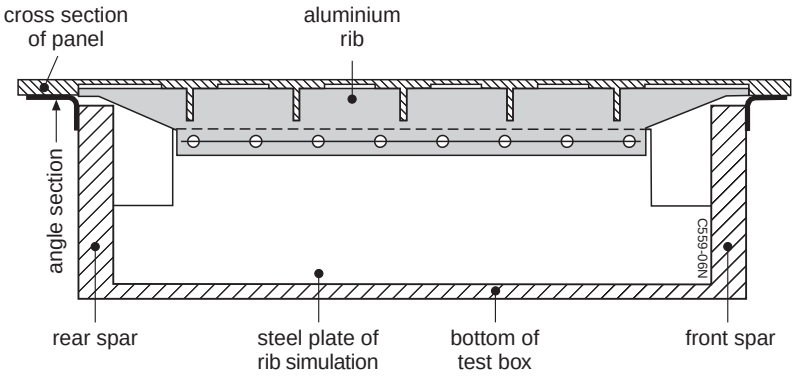

Fig. 4 Cross section of metal test box including a test panel

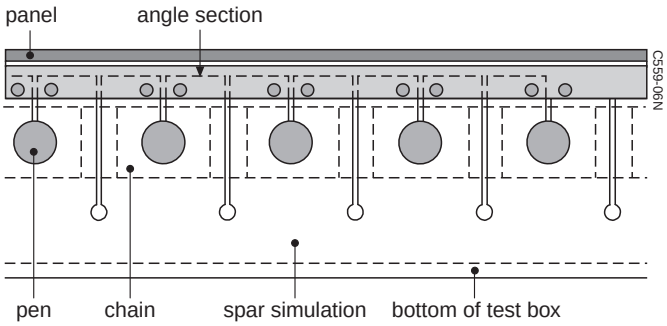

Fig. 5 Side view of the metal test box showing the slits in the steel spars

Fig. 6 Detail of the slit spar equipped with the chain

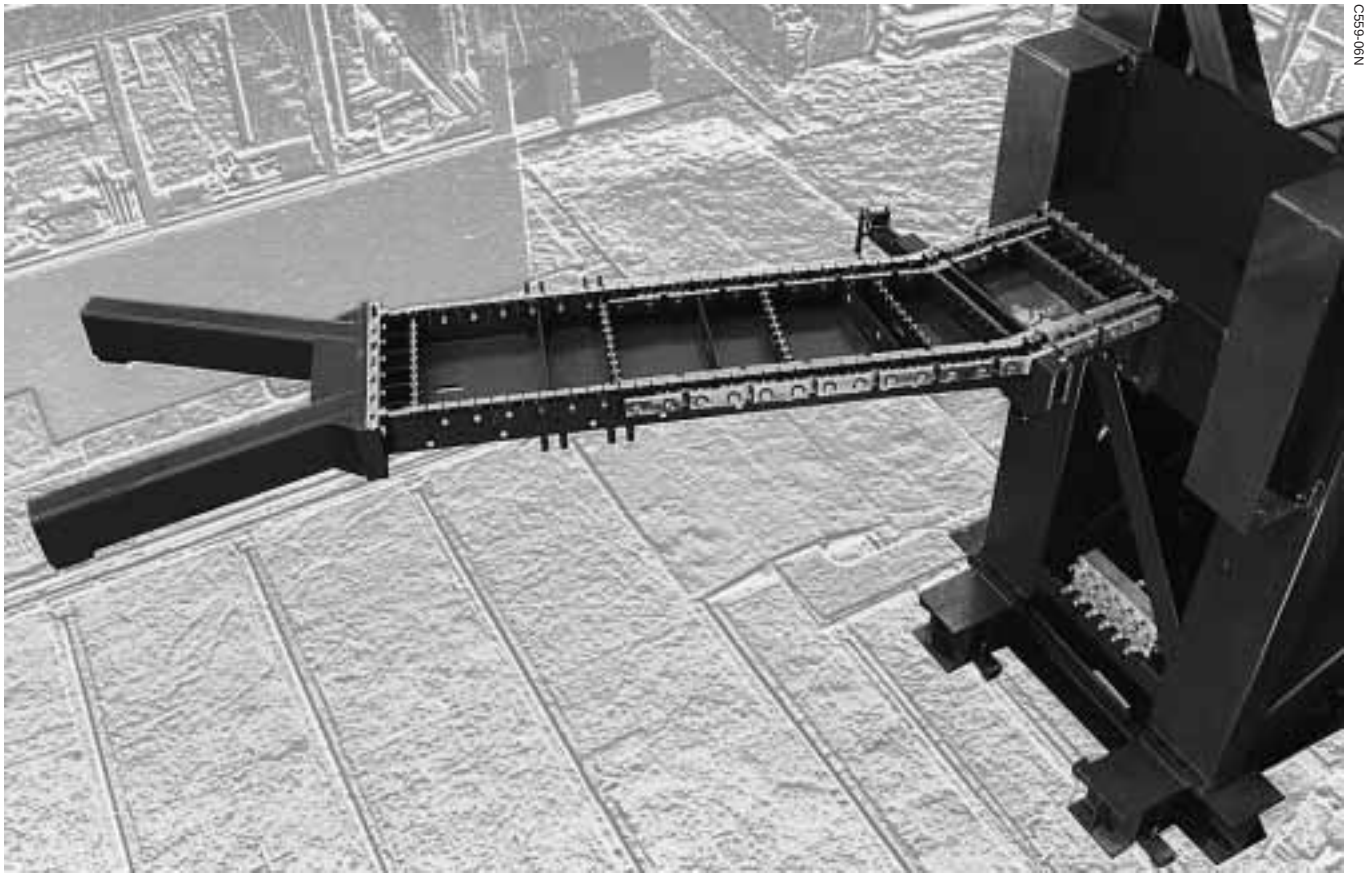

Fig. 7 Top view of the metal test box

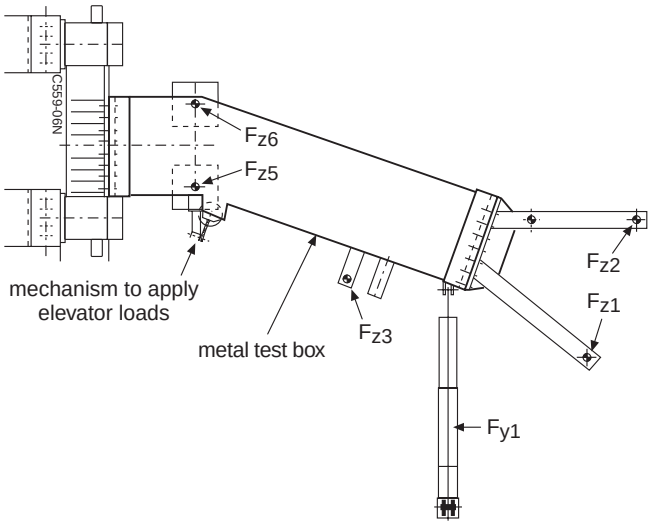

Fig. 8 Top view of metal test box test set-up

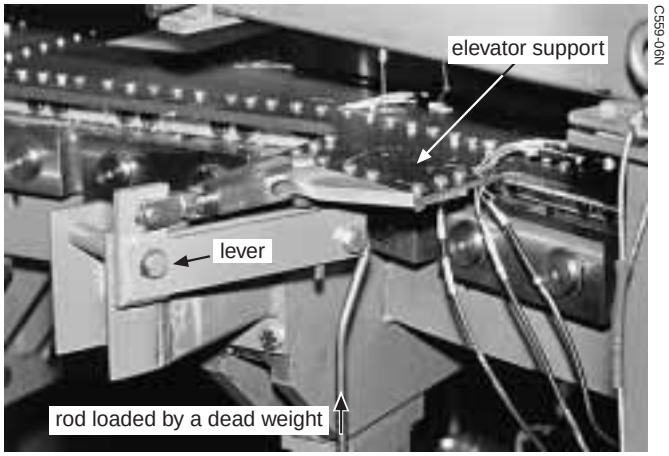

Fig. 9 Detail of mechanism used to apply elevator loads

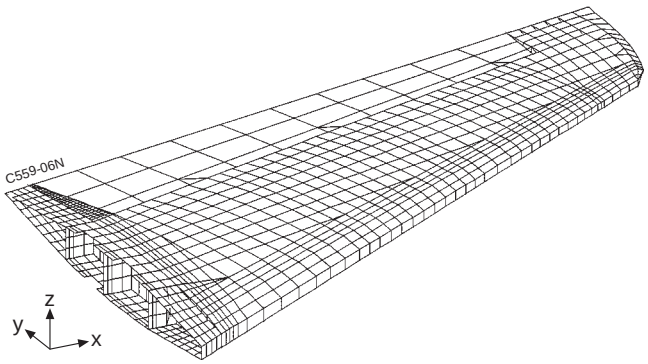

Fig. 10 Composite horizontal stabilizer finite element model

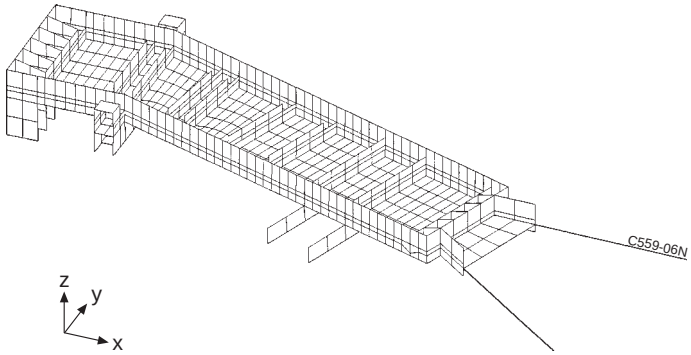

Fig. 11 Finite element model of test box

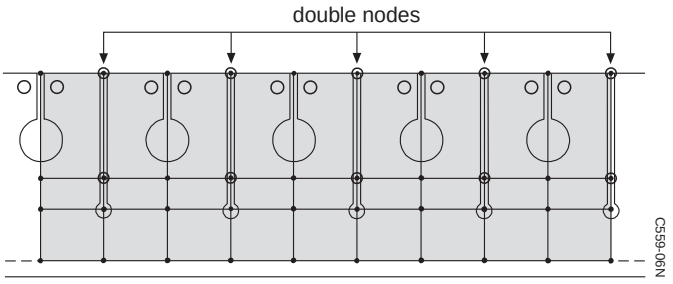

Fig. 12 Actual spar configuration and its finite element representation

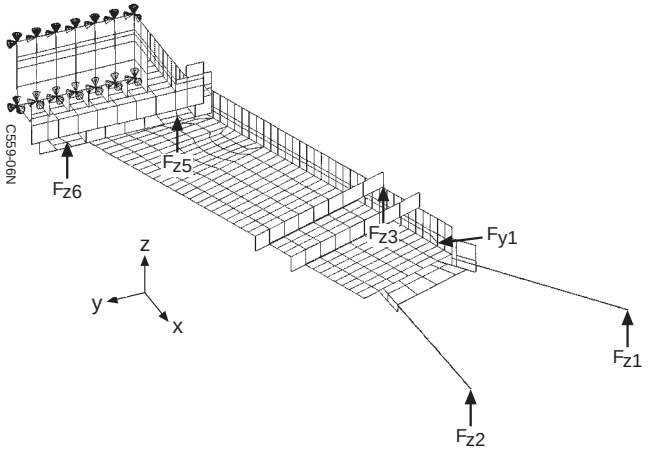

Fig. 13 Boundary conditions for test box finite element model

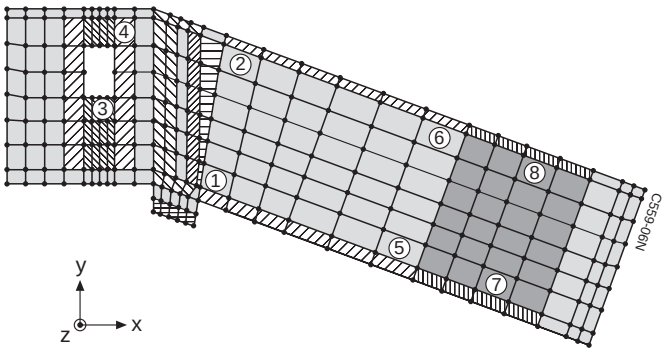

Fig. 14 Finite element model of Lower Aft panel, different fill patterns indicate different material properties, numbers indicate elements used in actuator load determination

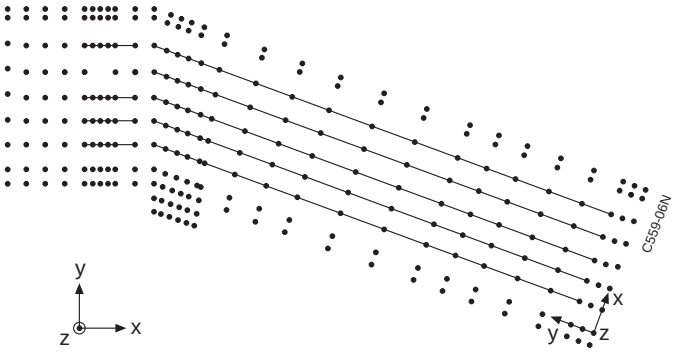

Fig. 15 Beam elements for Lower Aft panel

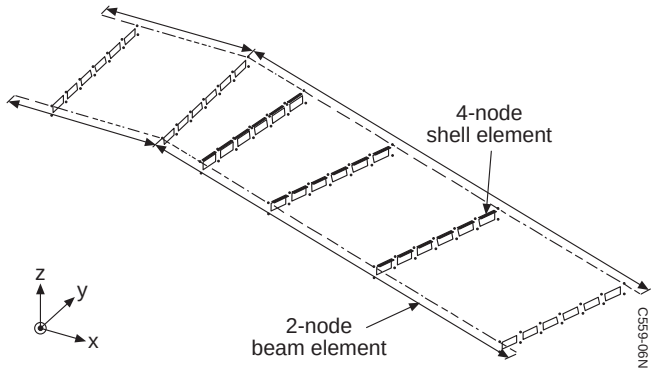

Fig. 16 Finite element model of the connection between panel and test box

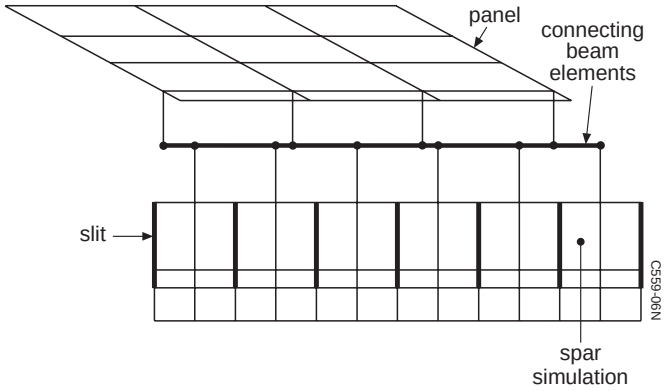

Fig. 17 Exploded view of connection between panel and spar simulation finite element models

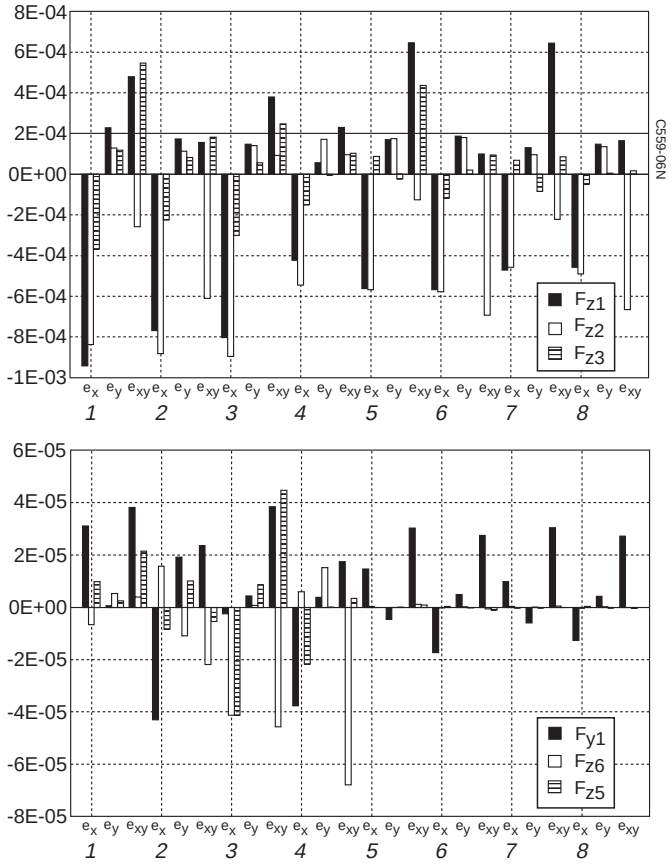

Fig. 18 Contributions of actuators to the strain distribution for Lower Aft panel

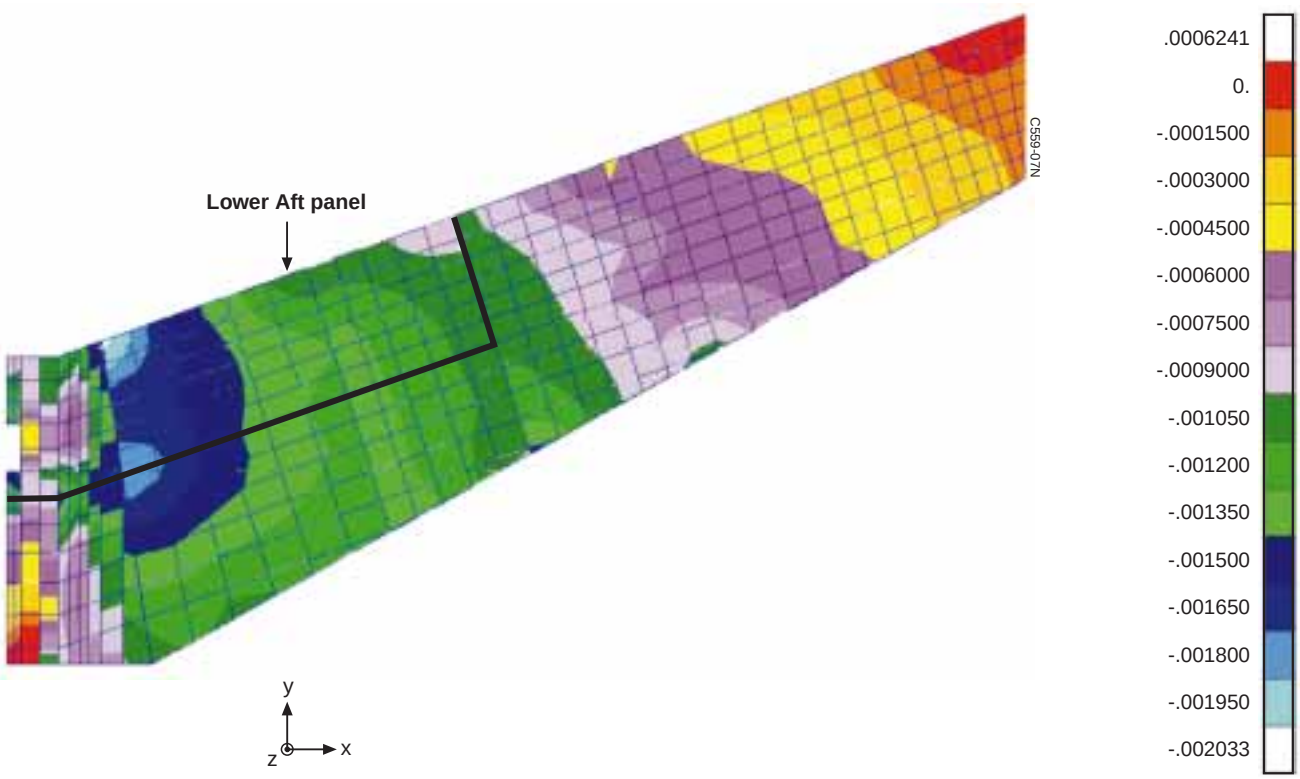

a) Stabilizer lower skin

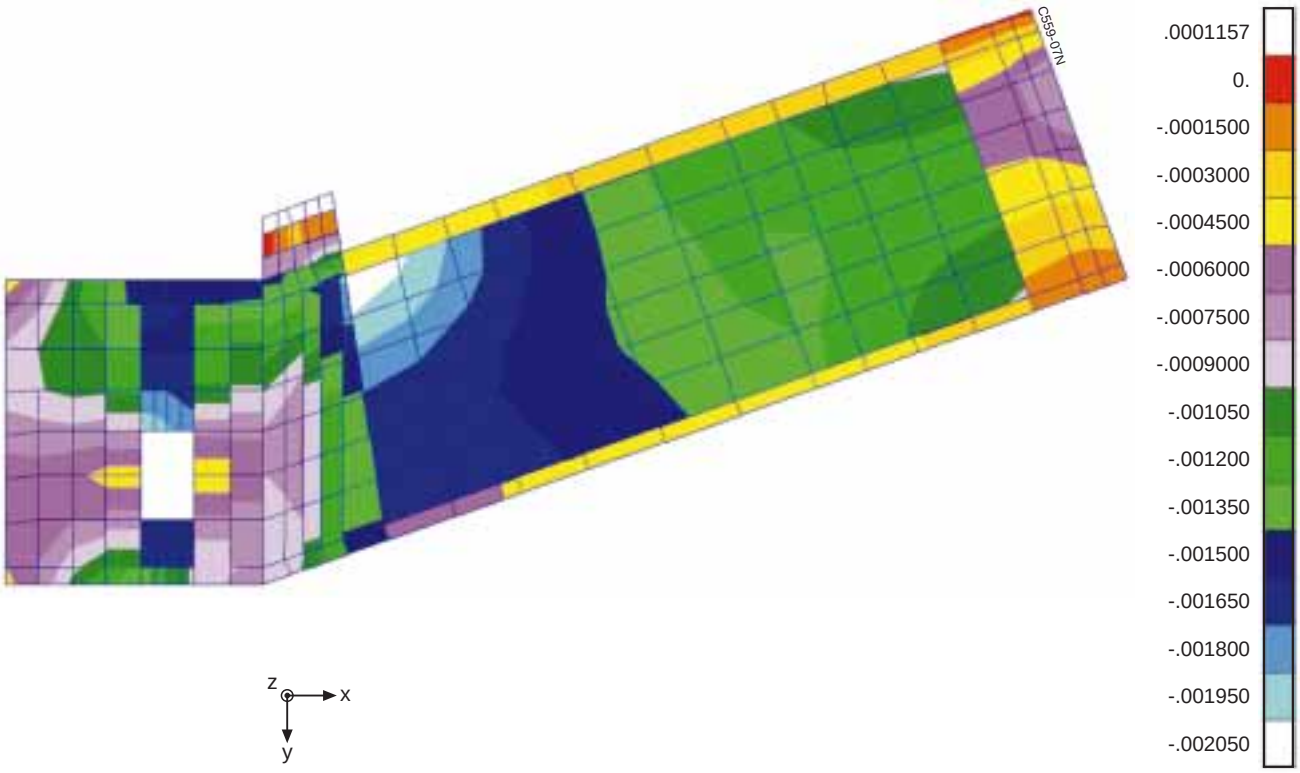

b) Lower Aft panel

Fig. 19 Strain in stringer direction

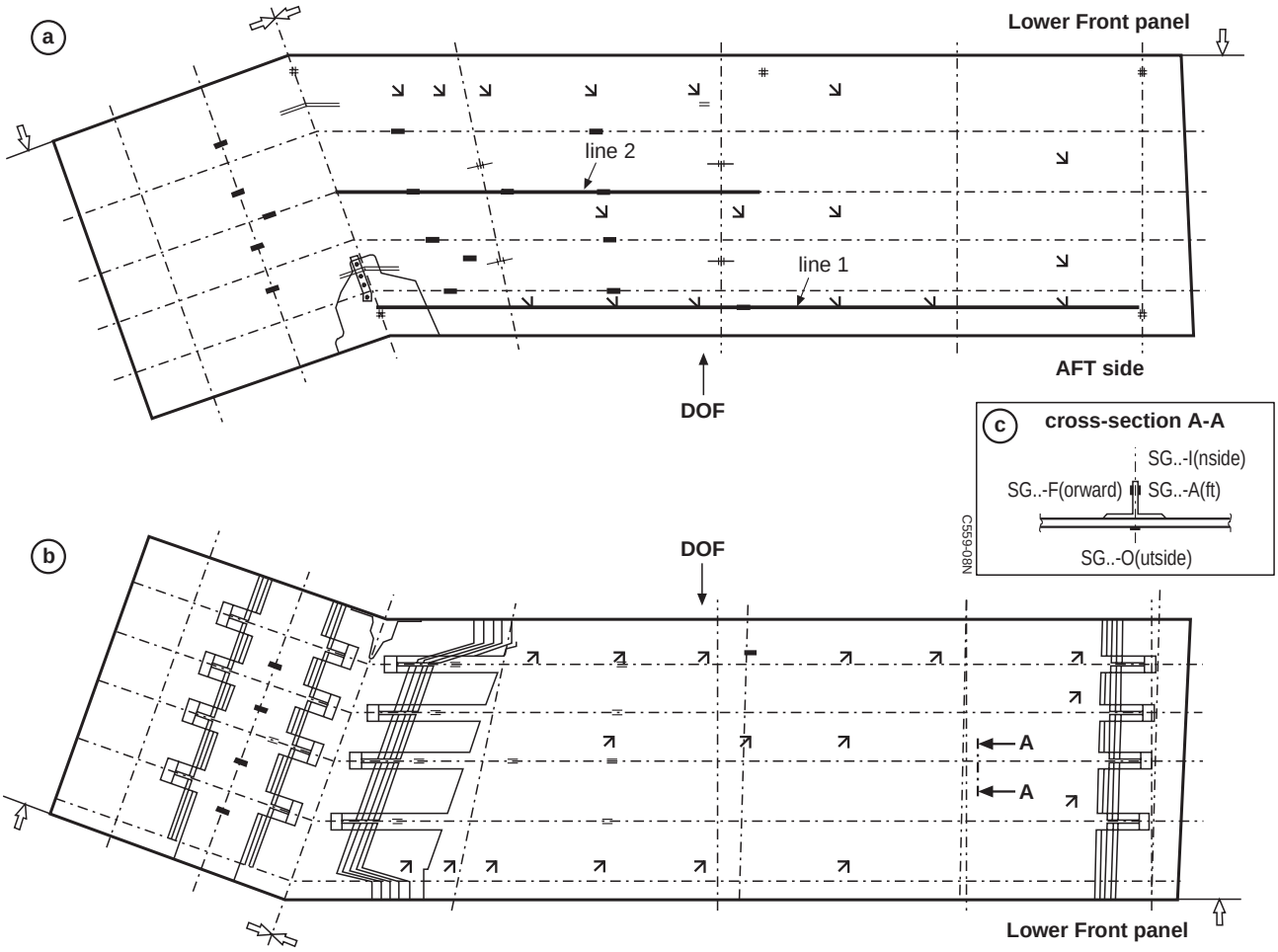

Fig. 20 Instrumentation plan of Lower Front panel

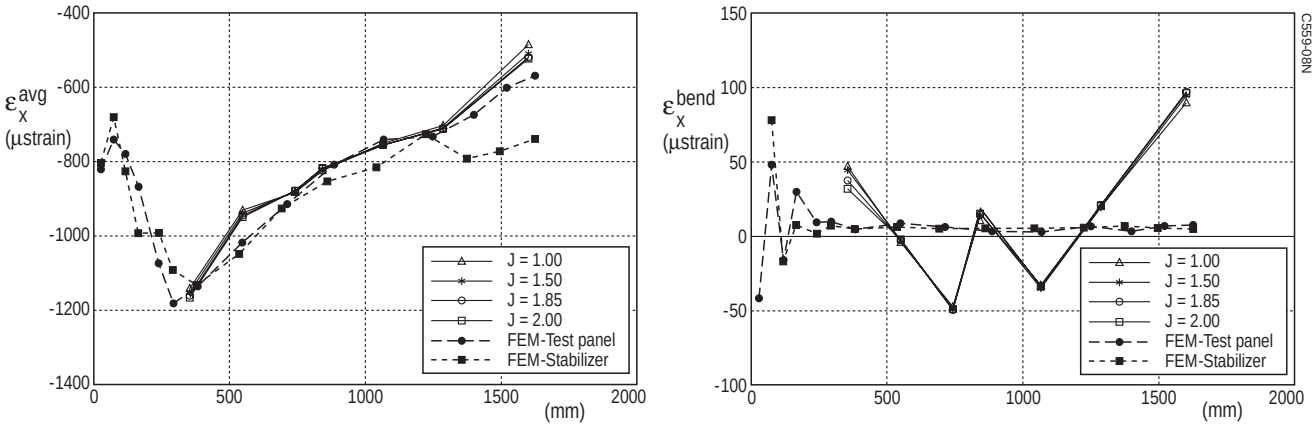

Fig. 21 Comparison of experimental and calculated scaled average and bending strains in stringer direction ε_x^{avg} and ε_x^{bend} (J = load factor)

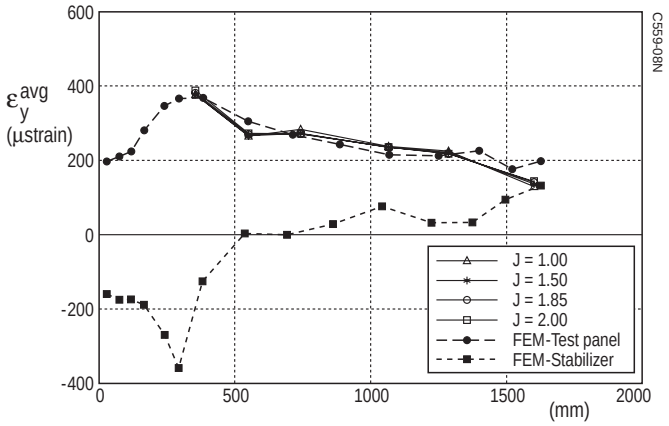

a) Scaled average strains perpendicular to the stringer direction ε_y^{avg}

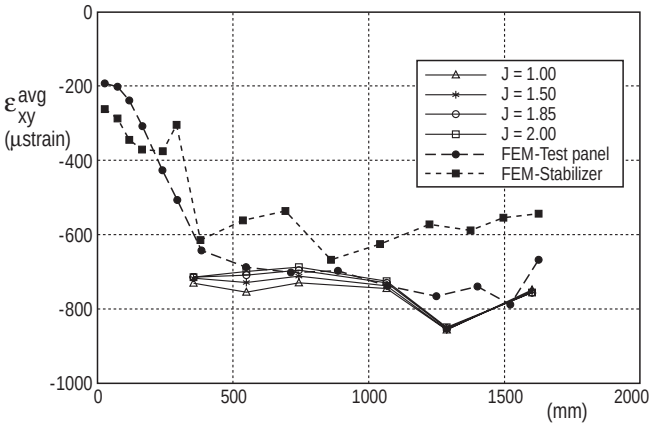

b) Scaled average shear strains ε_{xy}^{avg}

Fig. 22 Comparison of experimental and calculated scaled average strains

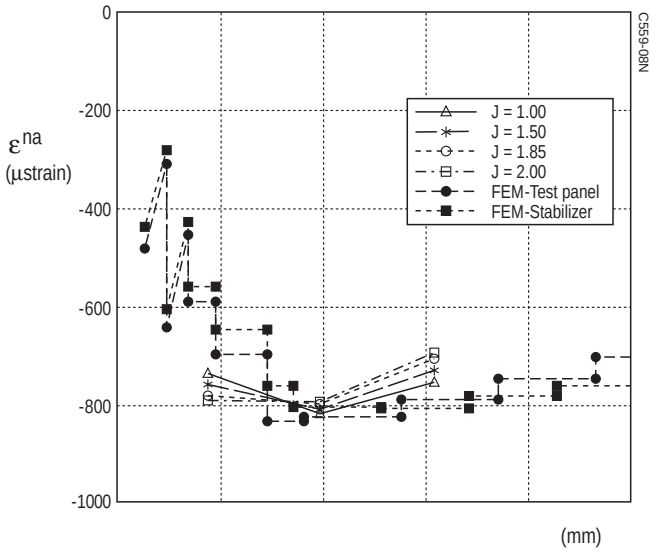

Fig. 23 Comparison of experimental and calculated scaled strain at the neutral axis of the stringer ε^{na}

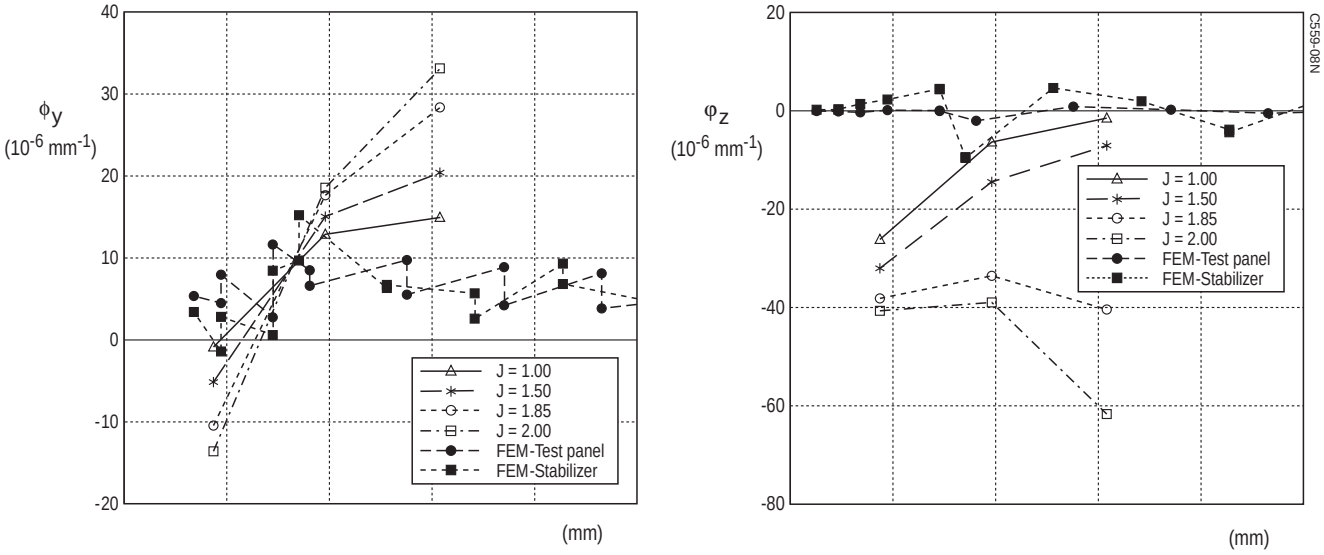

Fig. 24 Comparison of experimental and calculated scaled strain curvatures ϕ_y and ϕ_z